

# Formation of GM1 Ganglioside Clusters on the Lipid Membrane Containing Sphingomyeline and Cholesterol

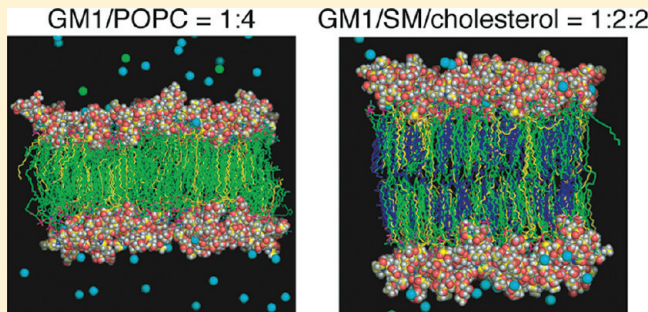
Kenichi Mori,<sup>†,§</sup> Md. Iqbal Mahmood,<sup>†</sup> Saburo Neya,<sup>†</sup> Katsumi Matsuzaki,<sup>‡</sup> and Tyuji Hoshino<sup>\*,†</sup>

<sup>†</sup>Graduate School of Pharmaceutical Sciences, Chiba University Inohana 1-8-1, Chuo-ku, Chiba 260-8675, Japan

<sup>‡</sup>Graduate School of Pharmaceutical Sciences, Kyoto University Sakyo-ku, Kyoto 606-8501, Japan

## Supporting Information

**ABSTRACT:** GM1 gangliosides form a microdomain with sphingomyeline (SM) and cholesterol (Chol) and are deeply involved in the aggregation of amyloid beta ( $A\beta$ ) peptides on neural membranes. We performed molecular dynamics simulations on two kinds of lipid bilayers containing GM1 ganglioside: GM1/SM/Chol and GM1/POPC. Both 10 and 100 ns simulations and another set of 10 ns simulations with different initial lipid arrangement essentially showed the same computational results. GM1 molecules in the GM1/SM/Chol membrane were condensed, whereas those in GM1/POPC membrane scattered. That is, the formation of GM1 cluster was observed only on the GM1/SM/Chol mixed membrane. There appeared numerous hydrogen bonds among glycan portions of the GM1 clusters due to the condensation. A comparison in distribution of lipid molecules between the two kinds of membranes suggested that cholesterol had important roles to prevent the membrane from interdigitation and to stabilize other lipids for interacting with each other. This property of cholesterol promotes the formation of GM1 clusters.



## 1. INTRODUCTION

Gangliosides are related to a wide variety of cellular functions like signal transduction. Some gangliosides have been rigorously studied in the fields of virus infections and nervous diseases.<sup>1,2</sup> A particularly well-known example is an interaction between the toxins secreted by *Vibrio cholerae*, which serves as a ligand, and monosialo-ganglioside (GM1 gangliosides) in intestine, which works as a receptor.<sup>3</sup> As for nervous diseases, gangliosides are involved in symptoms of many diseases of the brain such as Huntington's disease and Alzheimer's disease (AD).<sup>4–7</sup>

It was reported that the aggregation of amyloid  $\beta$ -peptides ( $A\beta$ ) in a human brain is an important risk factor for AD.<sup>8</sup> Moreover, recent studies have suggested that toxic  $A\beta$ s aggregate on lipid microdomains with highly condensed glycolipids (especially ganglioside), sphingomyeline (SM), and cholesterol (Chol).<sup>1,6,8,9</sup> A lot of evidence to indicate an essential role of cholesterol in AD was reported as described in the review by Shobab et al.<sup>10</sup> Yanagisawa et al. detected monosialoganglioside GM1-bound  $A\beta$  in the brains of patients with AD, and they suggested that the GM1- $A\beta$  complex might act as a seed for the aggregation of  $A\beta$ .<sup>11</sup> They hypothesized that there existed a particular kind of microdomain named as the detergent-insoluble glycosphingolipid-rich domain (DIG) and  $A\beta$ s were likely to be bound to DIG. Several in vitro studies have been carried out to clarify the lipid component of DIG and to examine the hypothesis.<sup>4–7</sup> Matsuzaki et al. demonstrated that high concentrations of cholesterol promoted the

formations of GM1 clusters and GM1- $A\beta$ ,<sup>6</sup> and they proposed that  $A\beta$  recognized the GM1 cluster. The interaction of  $A\beta$  with ganglioside-containing membranes was investigated by circular dichroism (CD) and Fourier transform infrared reflection (FTIR) spectroscopy, with comparison of the influence of the component of host lipid membranes among SM/Chol, POPC, etc.<sup>6</sup> The effect of lipid composition on the binding of  $A\beta$  to GM1-containing lipid bilayers was examined, preparing several kinds of DIG-mimicking lipid membranes<sup>9</sup> and also changing the species of ganglioside.<sup>12</sup> These experimental studies suggest that highly condensed GM1 molecules are critical for the formation of the GM1- $A\beta$  complex. An increase in Chol contents in the lipid bilayer enhanced the binding capacity of  $A\beta$  to the membrane and the lipid composition (GM1/SM/Chol = 1:2:2) is one of the adequate membrane providing DIG-like environments. The lipid membrane (GM1/POPC) is a good example to contrast with the DIG-like environment. Further, clarifying the molecular structure of the GM1 cluster is quite important to provide information for designing an inhibitor that blocks the interaction between GM1 and  $A\beta$ .

In this study, we performed molecular dynamics (MD) simulations on two types of GM1-containing membranes. One is comprised of GM1/d18:0-SM/Chol (composition is 1:2:2) and the other is of GM1/1-palmitoyl-2-oleoyl-sn-glycero-3-

Received: August 16, 2011

Revised: April 9, 2012

Published: April 12, 2012

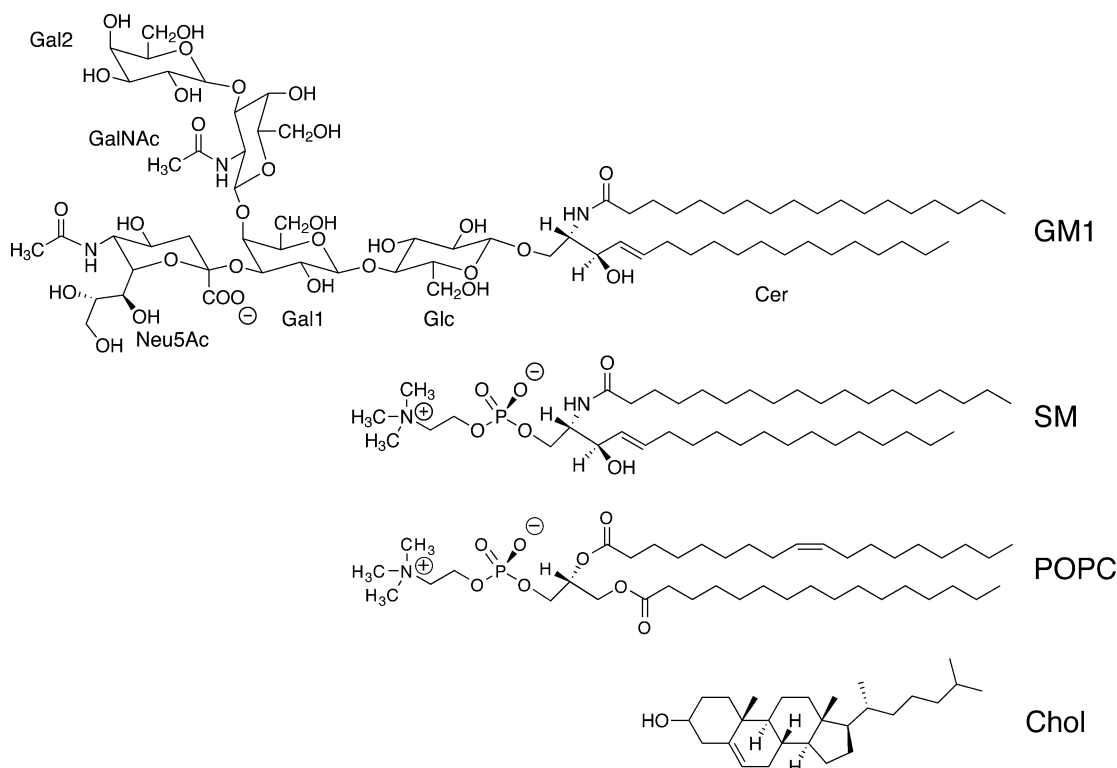


**Figure 1.** Chemical structures of the lipids used in the simulations.

phosphocholine (POPC) (composition is 1:4). These two kinds of lipid membranes, GM1/SM/Chol = 1:2:2 and GM1/POPC = 1:4, have been examined in detail in terms of the aggregation of  $\text{A}\beta$  peptides in the previous studies.<sup>6,9</sup> Comparative studies with changing the composition of the lipid membrane were also investigated by utilizing several kinds of analyzing techniques.<sup>12–14</sup> One of the techniques is a direct observation of surface morphology using an atomic force microscope (AFM).<sup>15</sup> The changes in morphology of GM1-containing membranes were observed using  $\text{GM1}_x/\text{SM}_{0.6-x}/\text{Chol}_{0.4}$  or  $\text{GM1}_x/\text{SM}_{0.5-x}/\text{Chol}_{0.5}$  membranes with changing  $x$ .<sup>13,14</sup> The phase separation was also examined with and without GM1 or SM in the Chol-containing membrane.<sup>16</sup> These AFM studies suggested that the morphology of the membrane surface is sensitive to a slight change in the lipid composition. Therefore,  $\text{A}\beta$  aggregation on the GM1/SM/Chol mixed membrane will be considerably influenced by the GM1 concentration. The lipid membranes GM1/SM/Chol = 1:2:2 and GM1/POPC = 1:4 were already well-studied in experiments. The former (GM1/SM/Chol = 1:2:2) is a typical lipid composition that causes  $\text{A}\beta$  aggregation. On the other hand,  $\text{A}\beta$  aggregation scarcely occurs on the latter (GM1/POPC = 1:4). Accordingly, it is interesting to contrast the conformation of GM1 molecules on these two kinds of membranes.

The computer simulations performed in this work will clarify what structure the GM1 cluster has and provide a clue to understanding the assembly of  $\text{A}\beta$  on GM1-containing cholesterol-rich membranes. We had developed a software program for modeling various types of lipid membranes,<sup>17</sup> and the software was utilized to build the initial structures for MD simulations. The model systems were created as close to experimental conditions as possible (lipid composition, temperature = 310 K, and ion concentration = 150 mM

NaCl). The lipid composition of GM1/SM/Chol has been often used as a raft-mimicking environment in many experimental studies.<sup>8,9,18–20</sup> Therefore, the results of our simulations will be helpful to understand the molecular structure of the raft-mimicking membrane as well as that of the GM1 cluster. For comparison, we also present the results of MD simulations on their counterpart without GM1, consisting of d18:0-SM/Chol and also POPC only. Several MD simulation studies have already been reported on the ganglioside-containing membranes or micelles.<sup>21–24</sup> The computational findings in those reports were closely linked to the experimental measurements, and then, the MD simulations provided important insights for interpreting experimental data. Our simulation will be also informative for the better understanding of ganglioside-containing mixed membranes.

## 2. METHODS

**Construction of the Initial Model Membranes.** The chemical structures of the lipids used in this study are shown in Figure 1. The electrostatic potentials of Chol and Neu5Ac were calculated by Gaussian 03<sup>25</sup> at the B3LYP/6-31+G\*\* level. The atomic charges were calculated by the RESP module of AMBER8.<sup>26</sup> The CHARMM force field for small organic molecules<sup>27</sup> and the CHARMM27 force field for lipids<sup>28</sup> were employed. All of the bilayer models were constructed using VMD<sup>29</sup> and an in-house program named GLYMM which is a VMD plug-in to implement a function to automatically generate a heterogeneous lipid bilayer.<sup>17</sup> The initial coordinates of all the lipids were built by the membrane tool in VMD, in which atom geometry was given in the liquid crystalline state of POPC. GLYMM converted the POPC bilayer into GM1/SM/Chol and GM1/POPC bilayers. The missing parameters were created based on the analogy with available parameters (List S1 in the Supporting Information).

A GM1/SM/Chol bilayer model consisted of 48 GM1, 96 SM, and 96 Chol molecules, and a GM1/POPC bilayer consisted of 48 GM1 and 192 POPC molecules. For comparison, SM/Chol and pure POPC models were also built. The replacement of glycan portions of GM1 molecules with choline phosphate groups resulted in the SM/Chol model, and the conversion of GM1 gangliosides of the GM1/POPC model into POPC resulted in the pure POPC model. The coordinates of the common portions were set equal. Water molecules were generated using the solvate program of VMD, which added pre-equilibrated water boxed around solute. About 20 000 water molecules were added to the respective bilayer models. Sodium ions were generated as counterions against the negatively charged GM1 molecules. The extra sodium ions and chloride ions were added so that the concentration of NaCl was equivalent to 150 mM.

**Detail Conditions of MD Simulations.** NAMD2.5<sup>30</sup> was used for MD simulations. The simulations were divided into five parts: minimization, heating, pre-equilibration, equilibration, and production runs. After the potential energy of the system was minimized, the system was heated to 310 K with the head groups of the lipids restrained, in which the lipids were allowed to move only in the *x* and *y* directions while their *z* coordinates were fixed. The pre-equilibration run was executed under the restraint. After gradually releasing the restraint, we equilibrated the system at a constant temperature and pressure (310 K and 1 atm). Finally the production run was carried out without any restraint and under the constant temperature and constant pressure condition. The calculation times for pre-equilibration, equilibration, and production runs were 10, 10, and 10, respectively. A periodic boundary condition was applied, and the pressure and temperature were kept constant by the Nosé-Hoover Langevin piston method. A cutoff distance for van der Waals and Coulomb potential forces at a real space was set to 12 Å. An integration time step was 2 fs. The particle mesh Ewald method was applied to incorporate the influence of long distance electrostatic force, in which the influence was computed at 4 fs intervals.

In order to examine whether the model membranes were equilibrated enough and the calculation results were independent of simulation time, we extended the simulation time up to 100 ns for one set of GM1/SM/Chol and GM1/POPC models. To avoid the dependency of the results on the initial arrangement of lipids, we executed another set of MD simulations both for GM1/SM/Chol and GM1/POPC. Each membrane model was constructed again with placing the lipid molecules at the different positions but with keeping the same lipid composition.

**Analysis of MD Simulations.** Calculation data were collected at 20 ps intervals during the last 5 ns for the 10 ns production runs and at 40 ps intervals during the last 50 ns for the 100 ns MD simulations. The thickness was determined from the distance between the averaged *z* coordinates of phosphorus atoms of the upper and the lower leaflets. The surfaces of the membranes were visualized by GRASP<sup>31</sup> to clarify the difference in morphology depending on the composition of the membrane. The order parameter was calculated by the following equation:

$$S_{CD} = \frac{3\langle \cos^2 \theta \rangle - 1}{2}$$

where  $\theta$  means the average angle between each of the C–H bonds of CH<sub>2</sub> groups of lipids and the bilayer normal vector (*z*

axis). The angle brackets denote average over time and over all lipids. Charge density distribution was obtained by counting partial charges in the sliced regions along the membrane normal direction. Hydrogen bonds (H-bonds) and radial distribution functions of charged atoms were calculated using ptraj module in AMBER8.<sup>26</sup> The criteria for H-bond is that the distance between heavy atoms is shorter than 3.5 Å and the angle of acceptor–hydrogen–donor configuration is larger than 120°. Further, using ptraj module, the H-bond occupancy was obtained as a percentage from probability of two atoms forming H-bond during the simulation. The average H-bond occupancy was calculated by dividing the sum of the occupancy by the number of molecules. In the measurement of H-bonds, oxygen atom was assigned as an acceptor and the nitrogen or oxygen atom having a bond to a hydrogen atom was defined as a donor. The number of water molecules along the membrane normal direction was counted in a thin layer whose width and depth were equal to *x* and *y* side lengths of the periodic boundary box and whose height in the *z* direction was 0.1 Å.

The probability density of lipids around Chol molecule was measured with respect to both distance and direction and was visualized using VMD. In order to account for the directional dependency of the molecular density around Chol, each coordinate of Chol in the respective trajectories was rotated and superimposed so that all the Chol molecules were fitted to the reference one. Grids with a spacing of 1.0 Å in *x*, *y*, and *z* directions were generated at the space around Chol. Then, the atoms of the specified molecules were counted at each grid for all the acquired Chol coordinates of all the trajectories and were averaged over trajectories and the number of Chols.

The above analyses were performed for two sets of 10 ns MD simulations on GM1/SM/Chol and GM1/POPC model membranes and also for 100 ns MD simulations of one set of GM1/SM/Chol and GM1/POPC models.

### 3. RESULTS

**Overall Picture of the Membranes.** Figure 2 shows snapshot structures of the two GM1-including bilayers after MD production run. The time-averaged thicknesses of GM1/SM/Chol, GM1/POPC, SM/Chol, and POPC bilayers were 46.0 ± 0.2, 34.7 ± 0.3, 49.5 ± 0.2, and 44.7 ± 0.3 Å, respectively. Interestingly, GM1/POPC showed interdigititation while POPC membrane did not. These results are compatible with the experimental results at 310 K that the membranes in the L<sub>O</sub> phase such as GM1/SM/Chol and SM/Chol are thicker than those in the L<sub>a</sub> phase such as POPC, and that the membranes in the L<sub>a</sub> phase are thicker than those in the interdigitated gel (L<sub>β</sub>I) phase such as GM1/POPC.<sup>32,33</sup> Therefore, the result of our simulation is reasonable in terms of membrane thickness. A large difference between GM1/SM/Chol and GM1/POPC was observed in area of membrane surface. The time-averaged areas of the GM1/SM/Chol and GM1/POPC were 4900 and 8010 Å<sup>2</sup>. Some clusters of glycans and some grooves between the clusters are observed in GM1/SM/Chol, whereas glycans of GM1 scatter around the membrane surface in GM1/POPC (Figure 2, panels b and c).

Figure 3 shows the distribution of GM1, SM, Chol, and POPC. As for GM1, GM1/SM/Chol shows sharper distributions of carboxyl and hydroxyl oxygen atoms of ceramide portion than GM1/POPC. In addition to the ceramide portion of GM1, the glycan residues except the terminal galactose (Gal2) have also sharper distribution in GM1/SM/Chol membrane. Interestingly, the distribution of the methylene

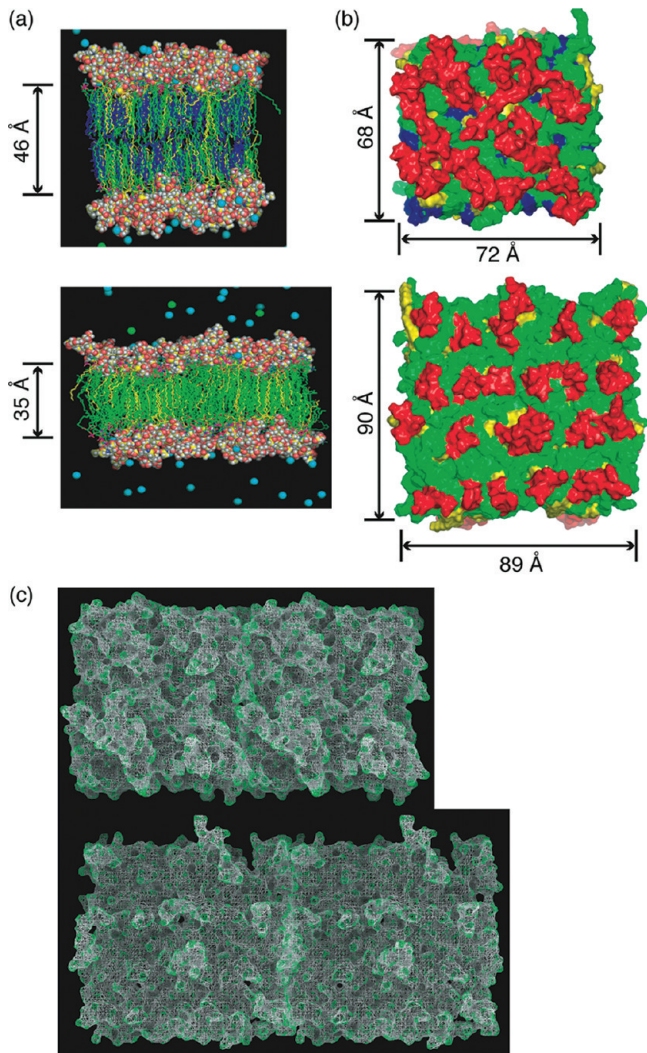


**Figure 2.** Snapshot structures of the membranes (upper, GM1/SM/Chol; lower, GM1/POPC). (a) Side views of the structures. Glycans of GM1 molecules and ions are represented as spheres colored by atom type, and the other lipids are drawn as sticks colored by residue type (green, SM or POPC; blue, cholesterol; yellow, ceramide part of GM1). The time-averaged thickness is shown in the left side. (b) Top views of the snapshot structures of the membranes colored by lipid type. Glycan portion of GM1 is colored red. The time-averaged  $x$  and  $y$  lengths of the membrane are shown in the lower and left sides. (c) Top views of the membranes colored by surface curvature. Periodic images of the unit cell are also shown so that continuous grooves between GM1 head groups can be recognized.

group of GM1 shows no local minimum at the center of the membrane in GM1/POPC (green lines in Figure 3). This characteristic distribution is due to the interdigitation of alkyl chains of the lipids. SM molecules in GM1/SM/Chol and SM/Chol membranes show quite similar distribution to each other. In contrast, the headgroup atoms of POPC in GM1/POPC have a broader distribution than those in pure POPC. This broad distribution is also due to the interdigitation of GM1/POPC membrane.

The order parameters,  $S_{CD}$ , of alkyl chains of the lipids in the two models were calculated from simulation data (Figure 4). The order parameters in GM1/SM/Chol are larger than those in GM1/POPC at almost all carbon positions, which indicates that the lipid alkyl chains in GM1/SM/Chol are aligned more

orderly than those in GM1/POPC. The order parameters for GM1/SM/Chol suggest that GM1/SM/Chol is in the  $L_o$  phase. The order parameters for SM and POPC of GM1/POPC are larger than those of GM1/SM/Chol at the terminal carbon positions, which indicates the interdigitation of lipids.

Figure 5 represents the number of water molecules measured along the surface normal direction and normalized relative to bulk. It is interesting to note that the diagrams show a complete sigmoid curve in the case of the absence of GM1 ganglioside, which suggests that GM1 has a strong influence on the distribution of waters. This calculation result is compatible with the findings by an experimental study using deuterium nuclear magnetic resonance ( $^2\text{H}$  NMR).<sup>34</sup> The  $^2\text{H}$  NMR measurement indicated two distinguishable water populations in the GM1 ganglioside micelles. This means that GM1 imposes a restriction on water dynamics and at least there exist two different environments for waters. One of the environments was suggested to be associated with the polar residues of GM1 headgroup. Further it is also notable that GM1/SM/Chol excludes more water molecules from the interface compared to the others. This water exclusion is due to high density of glycans at the membrane surface (Figure 3a). On the other hands, certain amounts of water molecules stay inside the top surface of GM1/SM/Chol. Interestingly GM1/SM/Chol and SM/Chol show the exactly same distribution of water molecules at the inside of membrane surface. Because the two bilayers contain the same ratio of Chol, this result suggests that the number of water inside the membrane surface may be a consequence of the presence of Chol molecules.

Figure 6 shows the charge density profiles along the membrane normal. Both profiles of the GM1/SM/Chol and GM1/POPC have large negative peaks at the membrane surface due to the phosphate moieties, following small positive peaks mainly due to the choline moieties of SM and POPC and partially due to the sodium ions diffusing from bulk. A clear difference is observed in the second large negative peak. There appeared a large second peak at the region distant from the surface in GM1/SM/Chol, whereas the corresponding peak almost diminished in GM1/POPC. This difference between GM1/SM/Chol and GM1/POPC is due to the change in distribution of Neu5Ac, while both models contain the same number of Neu5Ac residues. Neu5Acs in GM1/SM/Chol have a denser distribution on the membrane surface (Figure 2), and have a narrower distribution in the membrane normal direction (Figure 3) than those in GM1/POPC. This difference in the density of Neu5Ac is reflected in the second peak.

**Lipids Composition and Interaction.** In order to investigate the lipid–lipid interaction of the bilayers, H-bond occupancy was contrasted between lipids (Table 1). In GM1/SM/Chol, SM is more likely to form H-bonds with GM1 than with SM. The phosphate groups (PO<sub>4</sub>) and the ceramide backbones (NH, OH, and C=O; hereafter referred as Cer) are also involved in the H-bonds, the occupancies are not so large (Table 1, OH-PO<sub>4</sub> and NH-PO<sub>4</sub>). SM is prominently likely to form H-bonds between SM and glycan portion of GM1 instead of headgroup (see “SM-GM1” row and compare “Glycan” and “Head group” columns in Table 1). As for GM1-GM1, most of the H-bonds are between glycans, particularly at the terminal parts of glycans (Neu5Ac and Gal2). H-bonds between Cer-Cer are scarcely observed. In GM1/POPC, the most frequently observed H-bonds are between PO<sub>4</sub>-glycan, particularly between PO<sub>4</sub>-Glc. The glycan–glycan interaction among

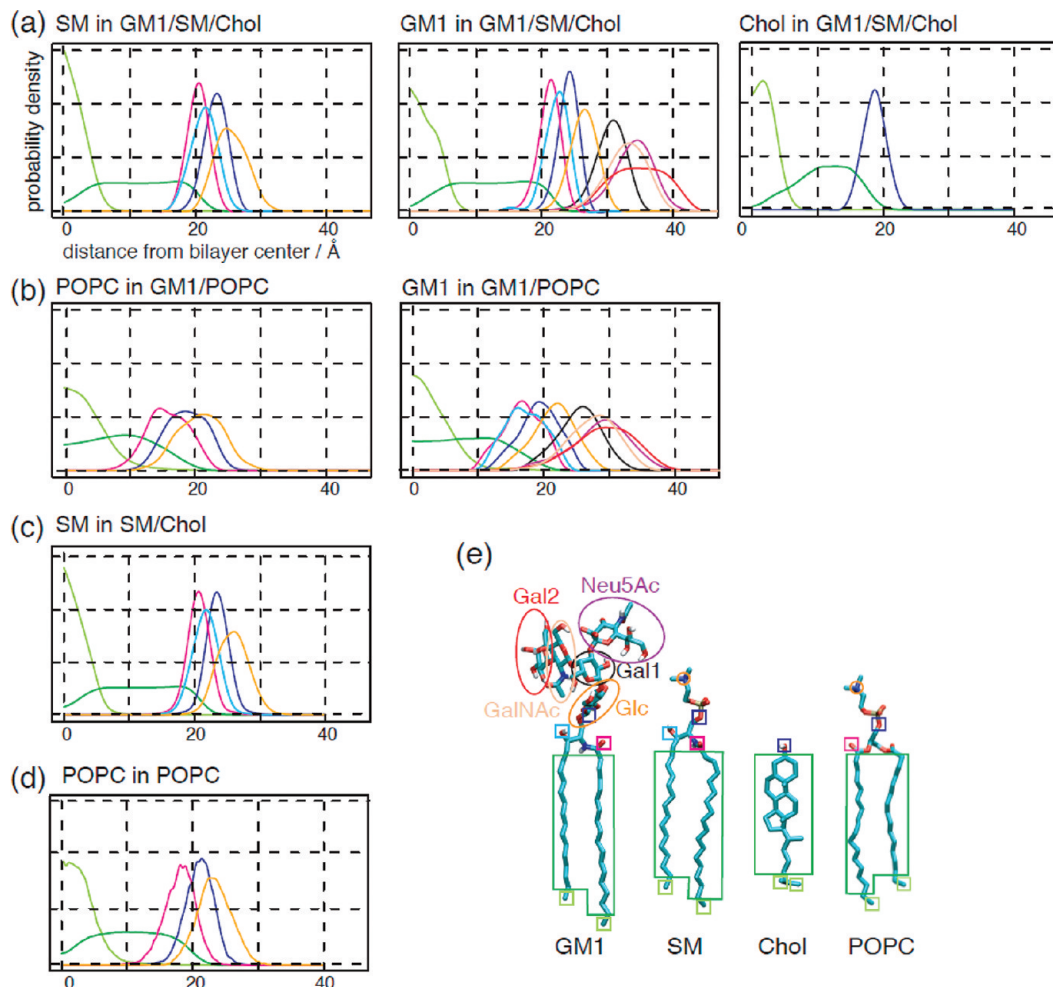


**Figure 3.** Probability densities of lipids measured along the membrane normal. Colors of the boxes and ovals on the molecules in panel e correspond to those for lines in panels a–d. (a) GM1/SM/Chol, (b) GM1/POPC, (c) SM/Chol, and (d) POPC.

GM1 molecules is also observed in GM1/POPC, but the occupancies are much less than those in GM1/SM/Chol.

According to the previous studies, cholesterol plays an important role in the formation of GM1 clusters.<sup>6,8,9</sup> Therefore, analysis of Chol interaction with other lipids is helpful to understand its role. Table 2 shows the H-bond occupancy between Chol and the other lipids. The occupancy of H-bonds between SM-Chol is three times larger than that of GM1-Chol, although the number of SM molecules is just twice as that of GM1. This result indicates that Chol tends to make H-bonds with SM rather than GM1. H-bonds between Chol-Chol are hardly observed.

The distribution of the tilt angle of Chol molecules resembles chi-square distribution. It is confirmed that Chol molecules in GM1/SM/Chol membrane keep their orientation almost perpendicular to the membrane surface. To investigate the Chol interaction in more detail, we analyzed the environment around Chol, in other words, the distribution of other molecules surrounding Chol (Figure 7a). The radial distribution function of the oxygen atoms of Chol shows the first peak at 5 Å (Figure S7). The distance indicates that Chol hardly has direct H-bonds with each other, which is consistent with the results of H-bond occupancy analysis. Figure 7b shows the distribution of GM1 and SM around Chol. As for GM1-Chol, the interaction shell around Chol reaches 15 Å, that is, the third shell appears at 15 Å apart from Chol. In contrast, the third

shell is barely observed for SM-Chol. This result indicates that GM1 arrangement is significantly affected by the presence of Chol. Judging from the high H-bond occupancy between GM1-GM1 (Table 1), GM1 molecules in the second solvation shell will attract the surrounding GM1 molecules, which results in the generation of the large third solvation shell.

**Characteristics of Glycans.** The interaction among the glycan portions of GM1 is focused as shown in Figure 8. A comparison of GM1/SM/Chol with GM1/POPC indicates a prominent increase in the intermolecular H-bonds among the terminal glycans (Neu5Ac and Gal2) and the GalNAc residues. On the other hand, no significant difference was observed in the intramolecular H-bonds. In both models, Gal1, the residue at the branching point of GM1, remarkably contributes to intramolecular H-bonds. A previous NMR experiment with GM1 micelles suggested that Neu5Ac formed intramolecular H-bonds with GalNAc.<sup>35</sup> In our simulation, intramolecular H-bonds between GalNAc-Neu5Ac are also frequently observed in both models. Taking both inter- and intramolecular H-bonds into account, it is concluded that Neu5Ac residue plays a quite important role to stabilize GM1 monomer and cluster conformations.

It was reported that the number of Neu5Ac of ganglioside was closely related to the aggregation of  $\text{A}\beta$ .<sup>6,7,36</sup> Moreover, our simulation indicated the importance of Neu5Ac in the GM1 containing membrane as shown in Figure 8. Hence, we

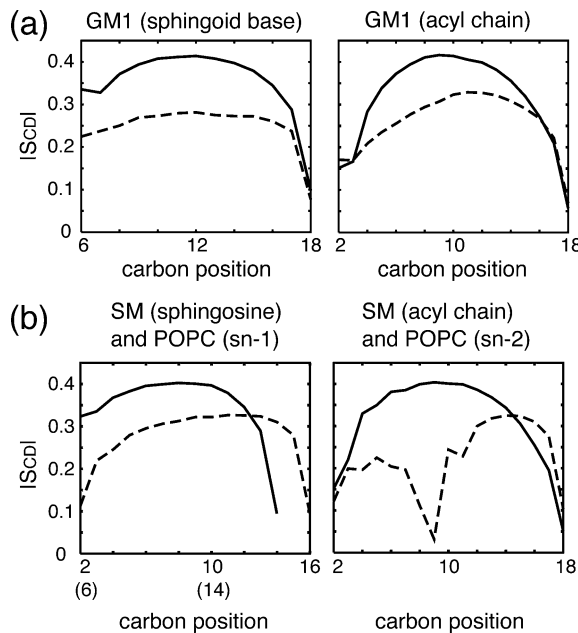


**Figure 4.** Order parameters of sphingosine and acyl parts of GM1, SM, and POPC. Solid and dashed lines show the results for GM1/SM/Chol and GM1/POPC, respectively. Parentheses in abscissa in panel b indicate the carbon position of sphingosine.

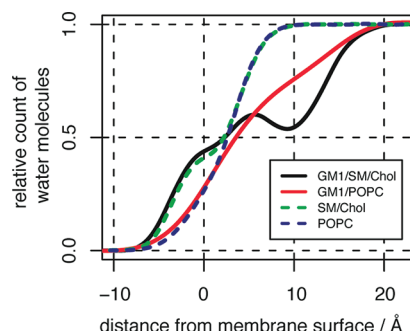


**Figure 5.** Normalized number of water molecules. The value in bulk water is set to 1.0. The zero position is determined from the maximum of the distribution of carbonyl oxygen atoms of lipid molecules in the respective bilayers.

hypothesized that the GM1 cluster would have a characteristic feature in the distribution of Neu5Ac and it might be involved in the mechanism of the aggregation. To analyze the

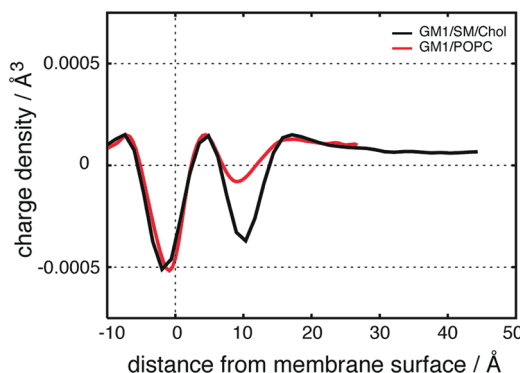


**Figure 6.** Charge density profiles along the membrane normal of GM1 ganglioside bilayers.

distributions of Neu5Ac, radial distribution functions (RDF) of carboxyl oxygen atoms of Neu5Ac of GM1 were examined (Figure 9). RDF of GM1/SM/Chol has a peak at 14 Å, whereas that of GM1/POPC shows a peak at 10 Å. Furthermore, the maximum value of the RDF of Neu5Ac in GM1/SM/Chol is 2.5-times larger than the bulk density, whereas that of GM1/POPC is no more than 1.5-times. This result indicates a high condensation of Neu5Ac in GM1/SM/Chol compared with GM1/POPC. A detailed view of the complex structure of glycans is shown in Figure 9b, where the distance between two Neu5Ac residues is 14 Å. GM1 molecules will produce dimer or cluster formations in this distance, and then the GM1 clusters are surrounded by numerous Chol molecules and SM lipids.

**Results of Additional Simulations with Other Initial Arrangements of Lipid and Results of Simulations Extended to 100 ns Production Run.** In order to check the dependency of the results on the initial GM1 arrangement, we carried out an additional set of MD simulations for GM1/SM/Chol and GM1/POPC membranes in which GM1 molecules were placed at the different positions at the starting point of the simulation. The results are shown in Figures S1–S5 and Tables S1–S2. As these figures and tables show, the second series of simulations gave similar computational results as the first ones. Therefore, we conclude that the findings from our simulation are independent of the initial arrangement of GM1 molecules.

We also performed 100 ns simulation for GM1/SM/Chol and GM1/POPC to check the dependency of the properties of model membranes on simulation time. The results are shown in Figures S7–S13. Because radial distribution functions, order parameters, distribution of lipid molecules, solvation of cholesterol, and charge density profile are almost consistent with those shown in Figures 3, 4, 6, 7, and 9, we conclude that the findings from our simulation are independent of the simulation time.

In Figures 3, S2, and S10, a large peak for SM head groups appears at the position over 20 Å measured from the center of the lipid bilayers for the GM1/SM/Chol membrane. In contrast, a peak for Chol head groups is observed at the position under 20 Å. The head groups of GM1 molecules are widely distributed in the range of 20–40 Å, and the peak positions of the respective residues appear in the order Glc, Gal1, GalNAc, NeuAc, and Gal2 from the lowest. In the GM1/POPC membrane, the peak positions for POPC head groups are mainly observed below 20 Å and GM1 head groups scatter broadly from 15 to 30 Å. These results are compatible among the 20 ns first and second simulations and also the 100 ns simulation. The radial distribution function of head groups of GM1 molecules has a peak at about 14 Å in GM1/SM/Chol mixed membrane as shown in Figure 9. This peak position is commonly seen in the 20 ns second simulation of Figure S5 and the 100 ns simulation of Figure S9. The presence of two large minima is a key feature in charge distribution along the direction of surface normal in the GM1/SM/Chol membrane. In contrast, the second minimum is quite small in the GM1/POPC membrane. This characteristic distribution is commonly observed in every result of the 20 ns first simulation of Figure 6, 20 ns second simulation of Figure S3, and 100 ns simulation of Figure S12. The interaction of Chol with GM1 is slightly stronger than that with SM. This strength is reflected in the formation of solvation shell around Chol in Figures 7b and S11(b). In the solvation shell of GM1 and Chol, the shell reaches 15 Å and a large amplitude is observed still in the third

Table 1. Hydrogen Bond Occupancy between Lipids<sup>a</sup>

		head group (without glycan, %)						glycan (%)				
		OH-PO4	OH-O=C	OH-OH	NH-PO4	NH-OH	NH-O=C	Glc	Gal1	GalNAc	Neu5Ac	Gal2
GM1/SM/Chol	SM-SM	6.8	1.1	0	1.8	2.1	1.8	NA	NA	NA	NA	NA
	SM-GM1	2.4	0.8	0.2	0.2	14.9	15.6	37.3	22.5	8.7	14.4	10.4
	GM1-GM1	NA	0.1	0.1	NA	0	0	24	10.2	18.9	19.9	29.1
GM1/POPC	POPC-POPC	NA	NA	NA	NA	NA	NA	NA	NA	NA	NA	NA
	POPC-GM1	11.9	NA	NA	16.7	NA	NA	47.1	20.7	31.2	20.3	27.2
	GM1-GM1	NA	0	NA	NA	0.6	0.0	21.1	5.3	10.8	3.4	6.7

<sup>a</sup>The occupancies are percentages of keeping the hydrogen bond for the last 5 ns of the simulation time. PO4 stands for the phosphate groups of SM and POPC. NH, OH, and O=C stand for the atoms at amide carboxyl group of the ceramide portion of GM1 and SM.

Table 2. Hydrogen Bond Occupancy between Lipids and Cholesterols<sup>a</sup>

	Cer-Chol	PO4-Chol	glycan-Chol
SM-Chol	15.1	11.2	NA
GM1-Chol	4.2	NA	4.7

<sup>a</sup>The occupancies are percentages of keeping the hydrogen bond for the last 5 ns of the simulation time. PO4 stands for the phosphate groups of SM. Cer stands a sum of NH, OH, and O=C at amide carboxyl group of the ceramide portion of GM1 and SM. Glycan represents oxygen and hydrogen atoms of glycan portion of GM1.

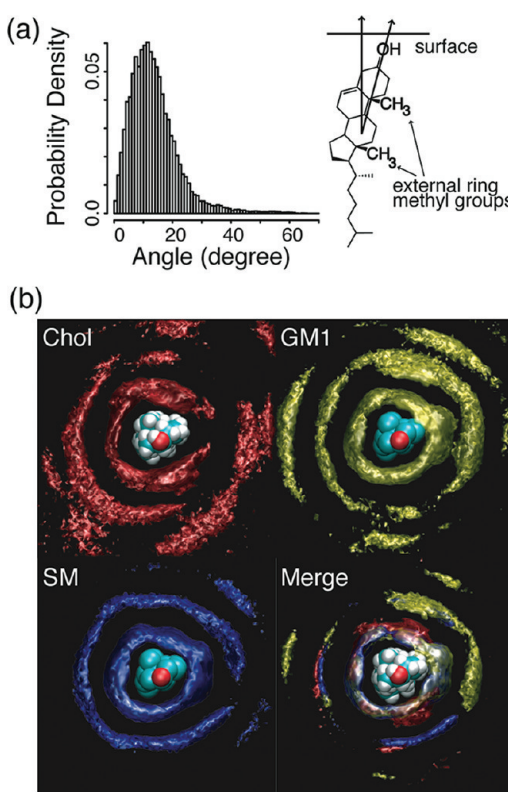


**Figure 7.** Orientation and solvation of cholesterol in the membrane. (a) Histogram of tilt angles of the principal axis of the Chol molecule with respect to the bilayer normal. Most probable orientation is shown in the right side. The membrane normal vector and the principal axis of Chol are also shown. (b) Distribution function of lipid chains around cholesterol with respect to distance and direction. The iso-surface plots are shown (red, Chol-Chol; yellow, Chol-GM1; blue, Chol-SM, hydrogen atoms are omitted for clarity in Chol-GM1 and Chol-SM). The merged iso-surface plot is shown at the lower right.

shell. On the other hand, the amplitude of the third shell is low for SM. This feature is also commonly observed in all of the simulations.

#### 4. DISCUSSION

**Effects of Sphingomyeline and Cholesterol on GM1 Cluster Formation.** The effect of cholesterol on the property of lipid bilayers has been widely studied.<sup>37,38</sup> In the computational approach, Pitman et al. carried out a 20 ns MD simulation on a mixed membrane consisting of Chol and 1-stearoyl-2-docosahexaenoyl-sn-glycero-3-phosphocholine (SDPC) in a ratio of 1:3.<sup>37</sup> The tilt angles of Chol with respect to the bilayer normal and the distributions of lipids around Chol are compatible with our present results (Figure 7). Although many experimental studies about raft microdomain have been reported, computational study on raft is limited. Niemelä et al. carried out 100 ns MD simulations of raft-like model membranes composed of palmitoyl-SM, Chol, and POPC in the ratios of 1:1:1 and 1:1:2.<sup>38</sup> They showed that nanoscale heterogeneity of lipids was observed in such model membranes. According to their results, the thicknesses of Chol rich and poor regions were 44 and 35 Å. These values are consistent with our results that the time-averaged thickness of GM1/SM/Chol was  $46.0 \pm 0.2$  Å and that of GM1/POPC was  $34.7 \pm 0.3$  Å, which are reflected in a prominent difference in Figure 2a. Each thickness is also consistent with the experimentally measured value of an SM bilayer with Chol and a pure POPC bilayer, which are 46–56 Å and 35 Å.<sup>39</sup> Furthermore, Niemelä et al. showed that two-dimensional distribution function of the center of mass of Chol is about 6 Å, which is close to our result that the first peak of oxygen atoms of Chol is 5 Å. It should be noted that the above properties relevant to the influence of Chol are compatible among the calculations performed independently in spite of the difference in concentration of Chol and composition of lipids. This suggests that cholesterol can exert the effect on many types of lipids in a broad range of concentrations.

In view of structure, GM1/SM/Chol resulted in the L<sub>O</sub> phase, while GM1/POPC resulted in the interdigitated phase (Figures 2–4). Mehlhorn et al. reported that GM1 caused the interdigitation of many kinds of phosphor-glycerides including egg PC.<sup>33</sup> Moreover, Ryhänen et al. suggested that an increase in charge density on membrane surface was a factor to induce interdigitation of dimyristoyl-PC (DMPC).<sup>40</sup> Further, a study with electron microscope indicated that GM1 dispersed in POPC bilayers.<sup>41</sup> GM1/POPC in our study also shows interdigitation, while GM1/SM/Chol bilayer does not display interdigitation in spite of a large increase of charge density on membrane surface.

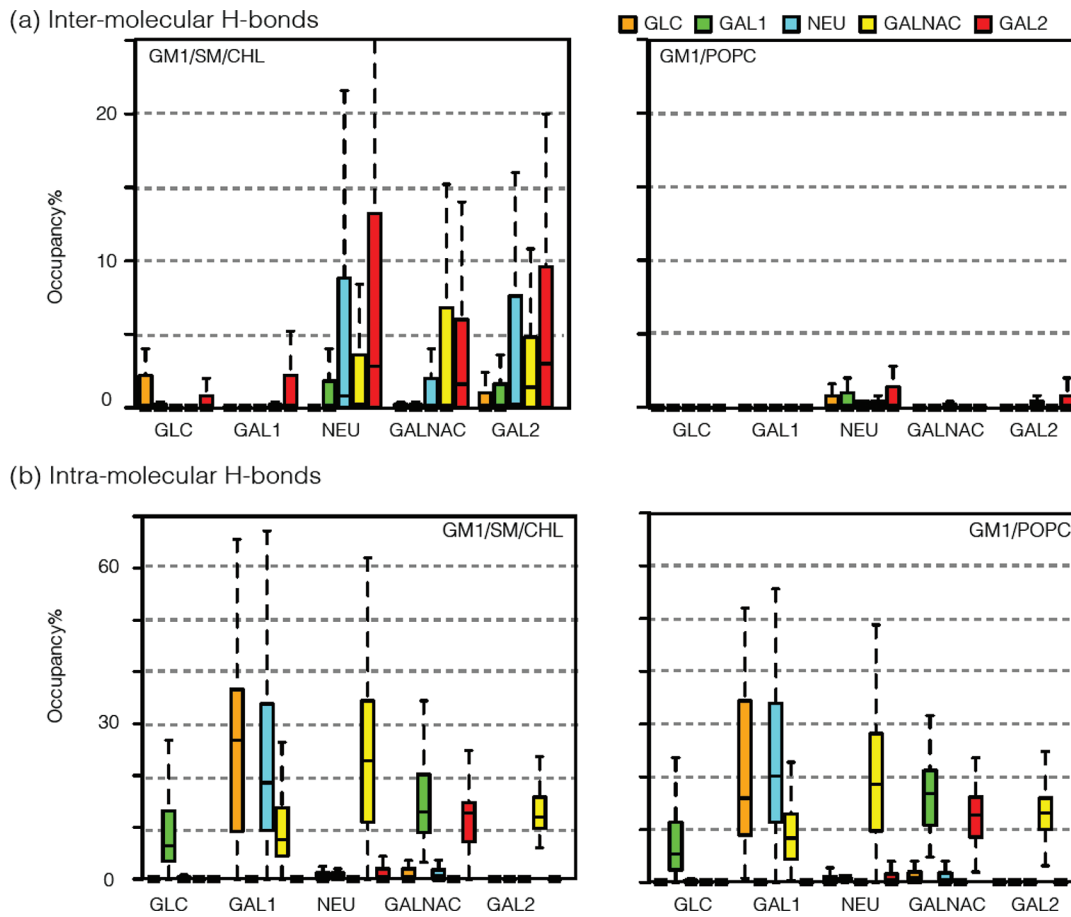


**Figure 8.** Boxplot of hydrogen bond occupancy between glycan residues observed for the last 50 ns. The plot indicates how often hydrogen bonds between the glycans were observed during the simulation. (a) Intermolecular hydrogen bonds between the glycan residues. (b) Intramolecular hydrogen bonds between the glycan residues. The residue names are shown in abscissa when they work as hydrogen bond donors. Glc, Gal1, Neu, GalNAc, and Gal2 are colored in orange, green, cyan, yellow, and red, respectively, when they work as hydrogen bond acceptor. The lower- and upper-bound of the box mean the first ( $Q_1$ ) and the third quartile ( $Q_3$ ), respectively. The midline of the box means median. The lower and upper whiskers of the boxplot mean the minimum and the maximum within  $Q_1 - 1.5$  times of the height of the box or  $Q_3 + 1.5$  times of the height of the box.

The time-averaged thickness of the GM1/POPC mixed membrane is small compared with the pure POPC. In pure POPC, the top surface of the membrane is flat. In contrast, the addition of GM1 molecules decreases the flatness of the top surface because Glc residue of glycan is partially buried in the membrane. This decrease in flatness enhances the overlap of alkyl chains of the upper and lower leaflets due to the release of steric hindrance of POPC head groups as shown in Figure S14. Further, the addition of GM1 to POPC enhances Coulomb repulsion between the anionic headgroup of GM1, which results in the expansion of an area of a bilayer. Interdigitation allows lipids in GM1/POPC to maximize the distance between the anionic head groups of GM1, resulting in minimization of the repulsion energy in their headgroup region. There would be no hydrogen bond formed directly between lipids in pure POPC membranes, as partially demonstrated in our work as shown in Table 1. On the other hand, the addition of GM1 remarkably increases the number of hydrogen bonds between lipids due to a number of hydrogen bond donors and acceptors of GM1 in the headgroup. Table 1 indicates that GalNAc, Neu5Ac, and Gal near the terminal of the glycan part of GM1 formed a lot of hydrogen bonds with POPC. This means that a lot of glycans lay on the surface of the membrane. Interdigitation allows the lipids to increase their distribution

range as shown in Figure 3, which promotes the formation of hydrogen bonds with the headgroup of POPC and reduces the repulsion among GM1 molecules. Incidentally, the distribution of saccharide residues is almost consistent with the results of the previous computational studies on GM1-containing dipalmitoyl-glycero-phosphatidylcholine (DPPC) and/or dioleyl-glycero-phosphatidylcholine (DOPC) membranes.<sup>23,24</sup> In the former membrane, the averaged vertical position of Glc was reported to be lower than that of phosphorus atoms,<sup>23</sup>

In the GM1/SM/Chol bilayer, the head groups of the lipids interact with each other through hydrogen bonding (Tables 1 and 2). Our results indicate that Chol is involved in the H-bond network (Table 2). Some previous studies have suggested that Chol has an effect of inhibiting interdigitation.<sup>42,43</sup> Chachaty et al. demonstrated using the synchrotron X-ray diffraction that Chol eliminated interdigitated phase in SM/Chol membranes,<sup>42</sup> and Tiemey et al. also indicated that Chol inhibited ethanol-induced interdigitation.<sup>43</sup> Interdigitation makes GM1 scatter around the surface as shown in Figure 2. Furthermore, Chol induces the generation of strong solvation shells by alkyl chains of SM and GM1 (Figure 7), which indicates that strong lateral attractive forces act on lipids. These lateral attractive forces will prevent the GM1 bilayer from interdigitating.

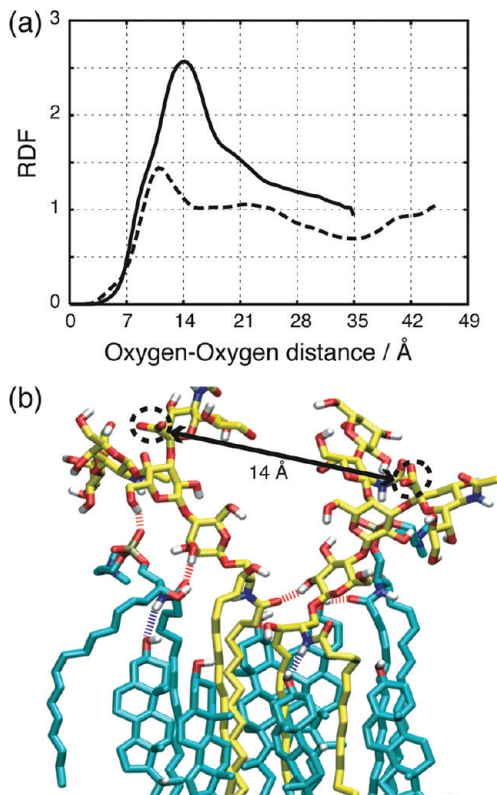


**Figure 9.** Distribution of Neu5Ac and snapshot structure of GM1/SM/Chol membrane. (a) Radial distribution functions of carboxy oxygen atoms of the Neu5Ac residue of GM1 in GM1/SM/Chol (solid line) and GM1/POPC (dashed line). (b) Snapshot structure of a GM1 dimer surrounded by Chol and SM. Nonpolar hydrogen atoms are omitted for visual clarity. The dashed lines represent the hydrogen bonds (red: OH-O, blue: NH-O). Carbon atoms of GM1 are colored yellow, and those of other lipids are colored cyan. Oxygen, nitrogen, and polar hydrogen atoms are colored red, blue, and white, respectively.

Therefore, SM and Chol provide an environment favorable for GM1 clustering in spite of the repulsive forces between GM1 molecules due to the negative charges.

**Characteristics of GM1 Cluster.** In GM1 clusters, a lot of intermolecular H-bonds are observed in this study (Table 1). A markedly large number of H-bonds are observed among the glycan portions of GM1, whereas those among the nonglycan head groups in GM1 are scarcely observed. The number of H-bonds among glycans of GM1 in GM1/SM/Chol is larger than those in GM1/POPC. This difference is prominent at the two terminal glycan residues, Neu5Ac and Gal2. The H-bonds contribute to the stabilization of GM1 clustering. Moreover, the clustering of glycans dehydrates the membrane surface of GM1/SM/Chol (Figure 5). Dehydration of a bilayer was reported to suppress the lateral diffusion of lipids.<sup>44</sup> In a rapidly diffusing situation, molecules have large kinetic energies, which prevents molecules from aggregation. Therefore, slow lateral diffusion due to dehydration can be a factor for GM1 clustering. Figure 3 shows that galactose and Neu5Ac residues are highly concentrated in the dehydrated region. Galactose has a hydrophobic face that can interact with hydrophobic or aromatic amino acid residues of proteins.<sup>45–47</sup> In addition, Neu5Ac carboxylic acid moiety produces a negatively charged region due to the GM1 clustering (Figure 6). The hydrophobic environment enhances the effect of hydrogen bonding.

Accordingly, GM1 clusters provide a stage favorable for interaction with a specific molecule containing some amount of H-bond donors and acceptors.

Some previous experimental studies suggested the importance of the concentration of Neu5Ac for  $\text{A}\beta$  binding to the ganglioside-containing membranes.<sup>4,6,36</sup> Our results indicates that Neu5Ac appears at the intervals of about 14 Å in GM1/SM/Chol (Figure 9 and also Figures S9). To examine structural relationship of this Neu5Ac distribution with amyloid peptides, we measured the distance between the amide nitrogen atoms of  $i$ th and  $(i + 1)$ th residues of amyloid peptides deposited in protein data bank (Figure S6). The histogram of the distances has a peak from 6.6 to 7.0 Å, which is almost compatible with half of the interval seen in the distribution of Neu5Ac. This suggests that  $\text{A}\beta$  in a  $\beta$ -strand conformation can recognize Neu5Ac residues aligned at a constant interval. That is, the alignment of Neu5Ac may facilitate the conformational change of  $\text{A}\beta$  into the  $\beta$ -strand from an  $\alpha$ -helix conformation, providing the stage suitable for specific H-bonds between Neu5Ac residues and peptides. In fact, an X-ray crystallographic structure of cholera toxin showed that cholera toxin recognized GM1 through H-bonds between main chain atoms of the toxin and Neu5Ac residues.<sup>3</sup> Furthermore, cholera toxin had a  $\beta$ -strand conformation at the interaction site.

**Properties of GM1 Molecules.** A study with nuclear magnetic resonance (NMR) spectroscopy provided significant information on the secondary structure and conformation of ganglioside micelles.<sup>48</sup> The inter-residue H-H nuclear Overhauser effect (NOE) was observed between the protons of ganglioside micelles. Since the hydroxyl and amide protons show distinct signals, the resonances of the protons provide the information for spatial connectivity. The NOE interaction was identified between Gal-OH and Gal-OH. This experimental observation is reflected in the hydrogen-bond interaction in Figure 8. In Figure 8, there appeared a stable hydrogen-bond between GLC and GAL1 both in the GM1/SM/Chol and GM1/POPC mixed membranes. This hydrogen-bond interaction is due to the OH group of GLC and that of GAL1 of ganglioside and these two groups are positioned close to each other.

A differential scanning calorimetry (DSC) measurement of dimyristoyl-glycero-phosphoryl-choline (DMPC) membranes with and without GM1 ganglioside indicated that the transition temperature between the gel and liquid-crystal phases increased due to the inclusion of GM1.<sup>49</sup> This increase of the transition temperature was also observed by Fourier transform infrared (FTIR) measurement. This suggests that hydrocarbon chains of DMPC/ganglioside membrane are more ordered than those of pure DMPC. This experimental suggestion is compatible with our simulation. The order parameters of the pure POPC are presented in Figure S15, for comparing those of the GM1/POPC membrane in Figure 4b. A comparison of the order parameters indicates that the alkyl chains, especially at the terminal regions, become more orderly aligned due to the inclusion of GM1 ganglioside molecules.

For investigating the lateral diffusion of lipids and Chol within the membrane plane, lateral diffusion constants,  $D_L$ , of GM1, SM, POPC, and Chol are calculated by the following equation:

$$D_L = \lim_{t \rightarrow \infty} \frac{1}{4t} \left\langle \sum_{\alpha} (\mathbf{r}_{\alpha}(t) - \mathbf{r}_{\alpha}(0))^2 \right\rangle$$

where the bracket means an ensemble average,  $r_a(t)$  represents the coordinate of the atom  $a$  at time  $t$ . The calculated  $D_L$  values of lipids in model membranes in Table S3 are consistent with the previous experimental results.<sup>50</sup> The  $D_L$  value of fluorescence-labeled GM1 molecules (10 mol %) in DMPC bilyars in liquid crystalline ( $L_\alpha$ ) phase at 308 K was measured to be  $0.47 \mu\text{m}^2/\text{s}$ ,<sup>51</sup> and the  $D_L$  of DMPC was  $1.6 \mu\text{m}^2/\text{s}$ . This experimental finding that the  $D_L$  value of GM1 is low compared with PC molecules is also compatible with our calculation. The  $D_L$  of pure DMPC was reported to be  $4 - 6 \mu\text{m}^2/\text{s}$  in  $L_\alpha$  phase<sup>52</sup> and about  $10^{-3} \mu\text{m}^2/\text{s}$  in gel phase.<sup>53</sup> Our simulation indicated that the incorporation of GM1 into a membrane in  $L_\alpha$  phase scarcely caused a drastic change in  $D_L$ , even though the GM1 incorporation makes a PC membrane interdigitated. In fact, the interdigitation was reported to hardly affect the translational diffusion of lipids.<sup>54</sup> Furthermore, our  $D_L$  value of POPC with 20 mol % GM1 in Table S3 is reasonable because the  $D_L$  of POPC in  $L_g$  phase was  $6.0 \mu\text{m}^2/\text{s}$  according to an NMR experiment.<sup>55</sup> In our simulations, the lipids in the liquid-ordered phase (GM1/SM/Chol) diffuse more slowly than those in the interdigitated phase (GM1/POPC). Judging from these consistencies of our results with the previous experiments, our simulations are considered to correctly reproduce the mixed lipid membranes.

In order to visually demonstrate the motion of head groups of GM1 gangliosides, animations were generated from the trajectory structures of the 20 ns first-round simulation both for GM1/SM/Chol and GM1/POPC membranes. The animations 1 and 2 in the Supporting Information correspond to GM1/SM/Chol and GM1/POPC, respectively. In the GM1/SM/Chol membrane, glycans were observed to move with dynamic displacement and to have many chances to be combined with each other. In contrast, glycans fluctuated in the respective local areas, and the displacement of glycans was relatively small in the GM1/POPC membrane. That is, the vigorous motion of GM1 head groups in the GM1/SM/Chol membrane increases the probability for the glycans of one GM1 molecule to be tightly bound to those of the other GM1 molecules, which results in the stable formation of clusters. Consequently, the number of intermolecular hydrogen-bonds in GM1/SM/Chol becomes larger compared with that in GM1/POPC as seen in Figure 8. Further, once glycan cluster is generated, lateral diffusion of lipids will be reduced because of the large mass-weight of clusters as shown in Table S3.

## 5. CONCLUSIONS

Molecular dynamics simulations were performed to investigate the formation of GM1 clusters on the lipid membrane. Two kinds of GM1-containing membranes, GM1/SM/Chol = 1:2:2 and GM1/POPC = 1:4, and their counterparts without GM1, SM/Chol and POPC, were modeled for simulation and the computational results were compared. The simulations presented the following findings. (1) GM1 cluster has hydrophobic and negatively charged surface due to the condensation of glycans, especially galactose and Neu5Ac. (2) Neu5Ac residues of GM1 appear at the intervals of about  $14 \text{ \AA}$  in GM1/SM/Chol, while they scattered around the membrane surface in GM1/POPC. (3) Hydrogen bond networks are formed among GM1 molecules and more hydrogen bonds are seen in GM1/SM/Chol membrane compared with GM1/POPC. (4) Cholesterol forms a lot of hydrogen bonds with GM1 and SM, and cholesterol plays important roles in

preventing the membrane from interdigitation and promoting other lipids to assemble.

## ■ ASSOCIATED CONTENT

### § Supporting Information

Hydrogen-bond occupancy, diffusion coefficients of lipids, force field parameters, and movies of MD simulations. Calculation results of the second and the extended 100 ns simulations are also provided in terms of distribution of lipid molecules, charge density profile, radial distribution function of oxygen atoms, order parameters of alkyl chains, etc. This material is available free of charge via the Internet at <http://pubs.acs.org>.

## ■ AUTHOR INFORMATION

### Corresponding Author

\*Phone: +81-43-226-2936. Fax: +81-43-226-2936. E-mail: hoshino@chiba-u.jp.

### Present Address

<sup>§</sup>Chemistry Research Laboratories., Drug Discovery Research, Astellas Pharma Inc., Miyukigaoka 21, Tsukuba, Ibaraki 305-8585, Japan.

### Notes

The authors declare no competing financial interest.

## ■ ACKNOWLEDGMENTS

This work has been supported by a Grant-in-Aid for JSPS fellowship and a grant from the Ministry of Education, Culture, Sports, Science and Technology, Japan. Calculations were performed at the Research Center for Computational Science, Okazaki, Japan and at the Information Technology Center of the University of Tokyo and also at Institute for Media Information Technology in Chiba University.

## ■ REFERENCES

- (1) Kimura, N.; Imamura, O.; Ono, F.; Terao, K. *J. Neurosci. Res.* **2007**, *85*, 2909–2916.
- (2) Suzuki, Y. *Prog. Lipid Res.* **1994**, *33*, 429–457.
- (3) Merritt, E.; Kuhn, P.; Sarfaty, S.; Erbe, J.; Holmes, R.; Hol, W. *J. Mol. Biol.* **1998**, *282*, 1043–1059.
- (4) McLaurin, J.; Franklin, T.; Fraser, P.; Chakrabartty, A. *J. Biol. Chem.* **1998**, *273*, 4506–4515.
- (5) Choo-Smith, L.; Garzon-Rodriguez, W.; Glabe, C.; Surewicz, W. *J. Biol. Chem.* **1997**, *272*, 22987–22990.
- (6) Matsuzaki, K.; Horikiri, C. *Biochemistry* **1999**, *38*, 4137–4142.
- (7) Ariga, T.; Kobayashi, K.; Hasegawa, A.; Kiso, M.; Ishida, H.; Miyatake, T. *Arch. Biochem. Biophys.* **2001**, *388*, 225–230.
- (8) Hayashi, H.; Kimura, N.; Yamaguchi, H.; Hasegawa, K.; Yokoseki, T.; Shibata, M.; Yamamoto, N.; Michikawa, M.; Yoshikawa, Y.; Terao, K.; Matsuzaki, K.; Lemere, C. A.; Selkoe, D. J.; Naiki, H.; Yanagisawa, K. *J. Neurosci.* **2004**, *24*, 4894–4902.
- (9) Kakio, A.; Nishimoto, S.; Yanagisawa, K.; Kozutsumi, Y.; Matsuzaki, K. *J. Biol. Chem.* **2001**, *276*, 24985–24990.
- (10) Shobab, L.; Hsiung, G.; Feldman, H. *Lancet Neurol.* **2005**, *4*, 841–852.
- (11) Yanagisawa, K.; Odaka, A.; Suzuki, N.; Ihara, Y. *Nat. Med.* **1995**, *1*, 1062–1066.
- (12) Kakio, A.; Nishimoto, S.; Yanagisawa, K.; Kozutsumi, Y.; Matsuzaki, K. *Biochemistry* **2002**, *41*, 7385–7390.
- (13) Mao, Y.; Tero, R.; Imai, Y.; Hoshino, T.; Urisu, T. *Chem. Phys. Lett.* **2008**, *460*, 289–294.
- (14) Shang, Z.; Mao, Y.; Tero, R.; Liu, X.; Hoshino, T.; Tanaka, M.; Urisu, T. *Chem. Phys. Lett.* **2010**, *497*, 108–114.
- (15) Frey, S. L.; Chi, E. Y.; Arratia, C.; Majewski, J.; Kjaer, K.; Lee, K. Y. C. *Biophys. J.* **2008**, *94*, 3047–3064.

- (16) Mao, Y.; Shang, Z.; Imai, Y.; Hoshino, T.; Tero, R.; Tanaka, M.; Yamamoto, N.; Yanagisawa, K.; Urisu, T. *Biochim. Biophys. Acta* **2010**, *1798*, 1090–1099.
- (17) Mori, K.; Hata, M.; Neya, S.; Hoshino, T. *Chem. Bio. Info. J.* **2004**, *4*, 15–26.
- (18) Yamamoto, N.; Hasegawa, K.; Matsuzaki, K.; Naiki, H.; Yanagisawa, K. *J. Neurochem.* **2004**, *90*, 62–69.
- (19) Kakio, A.; Yano, Y.; Takai, D.; Kuroda, Y.; Matsumoto, O.; Kozutsumi, Y.; Matsuzaki, K. *J. Pept. Sci.* **2004**, *10*, 612–621.
- (20) Yamamoto, N.; Matsuzaki, K.; Yanagisawa, K. *J. Neurochem.* **2005**, *95*, 1167–1176.
- (21) DeMarco, M. L.; Woods, R. J.; Prestegard, J. H.; Tian, F. *J. Am. Chem. Soc.* **2010**, *132*, 1334–1338.
- (22) Segà, M.; Vallauri, R.; Brocca, P.; Cantù, L.; Melchionna, S. *J. Phys. Chem. B* **2007**, *111*, 10965–10969.
- (23) Patel, R. Y.; Balaji, P. V. *J. Phys. Chem. B* **2008**, *112*, 3346–3356.
- (24) Jedlovszky, P.; Segà, M.; Vallauri, R. *J. Phys. Chem. B* **2009**, *113*, 4876–4886.
- (25) Frisch, M. J.; et al. *Gaussian 03*; Gaussian, Inc.: Wallingford, CT, 2004.
- (26) Case, D. A.; et al. *Amber 8*; University of California: San Francisco, CA, 2004.
- (27) Momany, F. A.; Rone, R. *J. Comput. Chem.* **1992**, *13*, 888–900.
- (28) Feller, S. E.; MacKerell, A. D. *J. Phys. Chem. B* **2000**, *104*, 7510–7515.
- (29) Humphrey, W.; Dalke, A.; Schulten, K. *J. Mol. Graph.* **1996**, *14*, 33–38.
- (30) Phillips, J. C.; Braun, R.; Wang, W.; Gumbart, J.; Tajkhorshid, E.; Villa, E.; Chipot, C.; Skeel, R. D.; Kale, L.; Schulten, K. *J. Comput. Chem.* **2005**, *26*, 1781–1802.
- (31) Nicholls, A.; Sharp, K. A.; Honig, B. *Proteins* **1991**, *11*, 281–296.
- (32) Ferrareto, A.; Pittó, M.; Palestini, P.; Masserini, M. *Biochemistry* **1997**, *36*, 9232–9236.
- (33) Mehlhorn, I.; Florio, E.; Barber, K.; Lordo, C.; Grant, C. *Biochim. Biophys. Acta* **1988**, *939*, 151–159.
- (34) Arnulphi, C.; Martin, C. A.; Fidelio, G. D. *Mol. Membr. Biol.* **2003**, *20*, 319–327.
- (35) Scarsdale, J. N.; Prestegard, J. H.; Yu, R. K. *Biochemistry* **1990**, *29*, 9843–9855.
- (36) Wang, S.; Rymer, D.; Good, T. *J. Biol. Chem.* **2001**, *276*, 42027–42034.
- (37) Pitman, M. C.; Suits, F.; MacKerell, A. D.; Feller, S. E. *Biochemistry* **2004**, *43*, 15318–15328.
- (38) Niemelä, P. S.; Ollila, S.; Hyvönen, M. T.; Karttunen, M.; Vattulainen, I. *PLoS Comput. Biol.* **2007**, *3*, e34.
- (39) Lodish, H.; Berk, A.; Matsudaira, P.; Kaiser, C. A.; Krieger, M.; Scott, M. P.; Zipursky, S. L.; Darnell, J. *Molecular Cell Biology*, 5th ed.; W. H. Freeman and Company: New York, 2003.
- (40) Ryhanen, S. J.; Alakoskela, J. M.; Kinnunen, P. K. *Langmuir* **2005**, *21*, 5707–5715.
- (41) Thompson, T. E.; Allietta, M.; Brown, R.; Johnson, M. L.; Tillack, T. W. *Biochim. Biophys. Acta* **1985**, *817*, 229–237.
- (42) Chachaty, C.; Rainteau, D.; Tessier, C.; Quinn, P.; Wolf, C. *Biophys. J.* **2005**, *88*, 4032–4044.
- (43) Tierney, K. J.; Block, D. E.; Longo, M. L. *Biophys. J.* **2005**, *89*, 2481–2493.
- (44) Gaede, H. C.; Gawrisch, K. *Biophys. J.* **2003**, *85*, 1734–1740.
- (45) Sujatha, M. S.; Balaji, P. V. *Proteins* **2004**, *55*, 44–65.
- (46) Sujatha, M.; Sasidhar, Y.; Balaji, P. *Biochemistry* **2005**, *44*, 8554–8562.
- (47) Chen, C.; Song, S.; Gilboa-Garber, N.; Chang, K.; Wu, A. *Glycobiology* **1998**, *8*, 7–16.
- (48) Acquotti, D.; Sonnio, S. *Methods Enzymol.* **2000**, *312*, 247–272.
- (49) Muller, E.; Giehl, A.; Schwarzmüller, G.; Sandhoff, K.; Blume, A. *Biophys. J.* **1996**, *71*, 1400–1421.
- (50) Filippov, A.; Oradd, G.; Lindblom, G. *Biophys. J.* **2003**, *84*, 3079–3086.
- (51) Goins, B.; Masserini, M.; Barisas, B. G.; Freire, E. *Biophys. J.* **1986**, *49*, 849–856.
- (52) Tocanne, J. F.; Dupou-Cezanne, L.; Lopez, A. *Prog. Lipid Res.* **1994**, *33*, 203–237.
- (53) Wu, E.; Jacobson, K.; Papahadjopoulos, D. *Biochemistry* **1977**, *16*, 3836–3841.
- (54) Schram, V.; Thompson, T. E. *Biophys. J.* **1995**, *69*, 2517–2520.
- (55) Lindblom, G.; Johansson, L. B.; Arvidson, G. *Biochemistry* **1981**, *20*, 2204–2207.